Title
Evolution of mechanical cooperativity among myosin II motors

Journal
Proceedings of the National Academy of Sciences of the United States of America, 118(20)

ISSN
0027-8424

Authors
Wagoner, Jason A
Dill, Ken A

Publication Date
2021-05-18

DOI
10.1073/pnas.2101871118

Peer reviewed

Evolution of mechanical cooperativity among myosin II motors

Jason A. Wagoner[a] and Ken A. Dill[a,b,c,1]

[a]Laufer Center for Physical and Quantitative Biology, Stony Brook University, Stony Brook, NY 11794; [b]Department of Chemistry, Stony Brook University, Stony Brook, NY 11794; and [c]Department of Physics and Astronomy, Stony Brook University, Stony Brook, NY 11794

Contributed by Ken A. Dill, April 2, 2021 (sent for review February 3, 2021; reviewed by Roger Cooke and David A. Sivak)

Myosin II is a biomolecular machine that is responsible for muscle contraction. Myosin II motors act cooperatively: during muscle contraction, multiple motors bind to a single actin filament and pull it against an external load, like people pulling on a rope in a tug-of-war. We model the dynamics of actomyosin filaments in order to study the evolution of motor–motor cooperativity. We find that filament backsliding—the distance an actin slides backward when a motor at the end of its cycle releases—is central to the speed and efficiency of muscle contraction. Our model predicts that this backsliding has been reduced through evolutionary adaptations to the motor's binding propensity, the strength of the motor's power stroke, and the force dependence of the motor's release from actin. These properties optimize the collective action of myosin II motors, which is not a simple sum of individual motor actions. The model also shows that these evolutionary variables can explain the speed–efficiency trade-off observed across different muscle tissues. This is an example of how evolution can tune the microscopic properties of individual proteins in order to optimize complex biological functions.

muscle | myosin | evolution | mechanobiology

Biomolecular machines are protein complexes that generate force, transport cargos, maintain ion gradients, and perform other functions throughout biology. Like macroscopic machines, biomolecular machines can be characterized by performance metrics like speed, efficiency, and power output. For many biomachines, evolution has optimized properties like speed and efficiency by tinkering with the machine's structure, binding affinities, or rates of internal transitions (1–4). Much work has gone into understanding these optimal mechanisms and the thermodynamic principles underlying them (1, 2, 5–9). The evolutionary trade-off between speed and efficiency for various molecular machines has also been studied (3).

Most of these prior works focus on how molecular motors are optimized as individual machines. Here, instead, we focus on how molecular motors are optimized to function collectively. To generate a muscle contraction, multiple myosin II motors must work together to pull an actin filament. It is not enough that the individual motors be fast and efficient; they must also coordinate their actions. Here, we study how evolution has optimized this coordination among myosin II motors.

We begin from the important experimental observation that myosin II transitions are force dependent (10). For example, Fig. 1 shows that the higher the load on a muscle fiber, the more myosin II motors are bound to actin (11). Like people pulling a rope in a tug-of-war, the more bound motors there are, the less force each motor must exert. The amount of force felt by an individual motor will depend on the forces exerted by all other motors. This gives rise to a force-mediated motor–motor cooperativity that affects not only the number of motors bound but also the order in which each motor performs its transitions.

It is reasonable to assume that this force-mediated cooperativity is optimizable through evolution. Then, what physicochemical properties of a motor can be altered to control this cooperativity, and what impact do these changes have on muscle speed and efficiency? We find that a key property of muscle contraction is how much an actin filament slides backward when a motor at the end of its cycle releases. The extent of this backsliding depends on how well the motors are coordinated. We identify different degrees of freedom of myosin II that appear to have evolved to minimize this backsliding. This also leads to an explanation of why fast, inefficient muscles have myosin II isoforms with a small force sensitivity, while slow, efficient muscles have isoforms with a high force sensitivity.

Myosin II Motors Must Work Cooperatively in Muscle Contraction

A half sarcomere, the basic unit of muscle tissue, consists of overlapping sets of thick (myosin) and thin (actin) filaments. During muscle contraction, multiple myosin II motors bind and perform work on an actin filament to drive the relative sliding of these two filaments past one another (12–15). Fig. 2 shows the chemomechanical cycle of an individual myosin II. The motor undergoes cycles of ATP hydrolysis in which it binds actin, pulls actin against the external load, and unbinds. Experiments show that myosin II is linearly elastic across its in situ function (16, 17), and therefore, the force exerted by a bound motor i is

$$f_i = k_{\mathrm{m}} y_i, \qquad [1]$$

where y_i is the strain and k_{m} the elasticity of myosin II.

Fig. 3 shows multiple motors working together in a half filament. When there are N motors bound to actin, the forces

Significance

Myosin II is a molecular motor that generates force and motion in muscle cells. During muscle contraction, many myosin II motors bind to the same actin filament, like people pulling on a rope in a tug-of-war. We study how myosin II motors have evolved to coordinate their actions. We find that a key property of muscle performance is how far a filament slides backward when a motor at the end of its cycle releases. This backsliding is not a property of an individual motor; it depends on the entire multimotor system. We find evidence that myosin II has evolved to minimize this backsliding. These evolutionary trends also explain differences in speed and efficiency observed in muscle tissues across different species.

Author contributions: J.A.W. and K.A.D. designed research; J.A.W. performed research; J.A.W. analyzed data; and J.A.W. and K.A.D. wrote the paper.

Reviewers: R.C., University of California San Francisco; and D.A.S., Simon Fraser University.

The authors declare no competing interest.

[1]To whom correspondence may be addressed. Email: dill@laufercenter.org.

This article contains supporting information online at https://www.pnas.org/lookup/suppl/doi:10.1073/pnas.2101871118/-/DCSupplemental.

Published May 11, 2021.

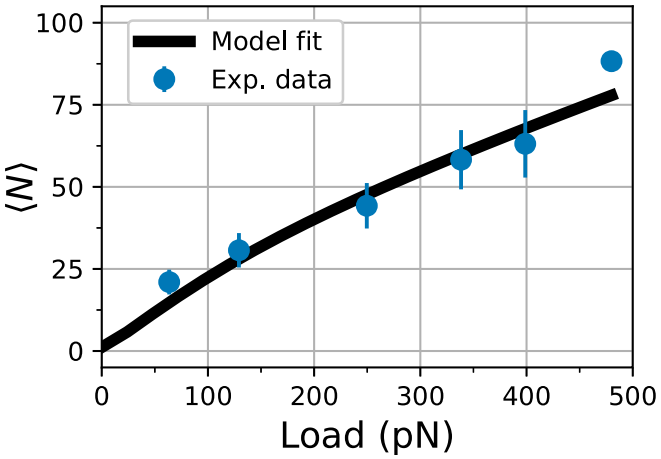

Fig. 1. Actomyosin needs more myosin II motors when there is a greater external load. As the load on the actin filament increases, the number of motors bound to actin $\langle N \rangle$ increases. Data from Piazzesi et al. (11) for a half filament with 294 total myosin II motors and isometric tension $F_0 = 480$ pN.

exerted by these motors must balance the external load F on the filament:

$$\sum_{i=1}^{N} f_i = F. \qquad [2]$$

When F is large, more motors are needed to counterbalance it, as demonstrated in the experimental measurements of Fig. 1.

Forces and strains vary across the bound motors. A motor initially binds in a pre-power stroke state that is weakly bound and does not generate force (18). When the motor releases phosphate and performs the power stroke, the lever arm swings a distance $d = 8$ nm (19), which is constant with respect to force. This stroke increases the force exerted by and the strain on the motor (Fig. 3, A $\rightarrow$ B). During the stroke, the actin filament is pulled to the left a distance $\Delta x_{\text{step}} = d/N$, where x is the position of the actin filament. Because the actin filament has moved, the strain on the other post-power stroke motors is relieved by the same amount, d/N. Therefore, motors in the post-power stroke state have a range of strain values (Fig. 3). A motor just after its power stroke will have a large strain but will become increasingly unstretched as other motors perform their strokes and the actin filament slides to the left.

When a post-power stroke motor unbinds from the actin filament, the actin filament will slip backward a distance proportional to that motor's strain $\Delta x_{\text{slip}} = y_i/(N-1)$ until the $N-1$ remaining motors "catch" the actin filament (Fig. 3, B $\rightarrow$ C). When a person exits a tug-of-war, the rope will slip toward the other team. The net productive motion or stroke size achieved by a motor is $\Delta x_{\text{net}} = \Delta x_{\text{step}} - \Delta x_{\text{slip}}$.

To reduce filament backsliding, it is better if the post-power stroke motors release in a particular order, so that those that have been bound longest—which have the smallest strain and slip distance Δx_{slip}—release first. To do this, myosin II motors must act cooperatively, which they accomplish through force-sensitive states and transitions. Eq. **2** shows that the force felt by an individual motor depends on the external load F and on the forces exerted by all other motors. Therefore, force sensitivity allows a myosin II to coordinate its actions with the actions of other bound motors.

Although it is not completely known which transitions of Fig. 2 are force dependent (10), experiments and models show that ADP release from myosin becomes slower as the force or strain becomes larger (10, 17, 20–25). This step is rate limiting, and the subsequent ATP binding is very fast under physiological concentrations. So, the force dependence of ADP release controls the motor's release from actin (17). We model the motor off rate from actin as (24, 25)

$$\omega_{\text{off, i}} = \omega_{\text{off}}^0 e^{-\beta\delta f_i}, \qquad [3]$$

where ω_{off}^0 is the rate at zero force, $\beta = 1/kT$, and the force dependence $\delta > 0$ expresses that a larger force leads to a slower off rate. Because the force f_i is proportional to the strain y_i, which in turn is proportional to the slip distance Δx_{slip}, it means that those motors having the smallest strain and smallest slip distance will have the fastest off rates.

A Model for the Speed and Efficiency of Muscle Contraction over Evolutionary Degrees of Freedom

We construct a model of actomyosin that captures the details given in the previous section; full details are given in *SI Appendix*, section 1. We have drawn on insights gained from other actomyosin models (24, 26, 27), particularly those of Lombardi and coworkers (17, 28, 29)—a more detailed model that requires numerical simulation—and the parallel cluster model (30, 31)—one that attains an analytical solution by assuming a separation of timescales for myosin II transitions and that all bound motors have equivalent strain. Our model is unique in that it contains the detail necessary to capture the average distribution of strain across bound motors while also being analytically solvable.

We model an actomyosin filament with N_{T} active myosin II motors. Each motor is in one of five possible states. Compared with the cycle shown in Fig. 2, our model does not explicitly include the rigor state and includes an intermediate state along the power stroke (labelled "mid-power stroke") (24), which has been experimentally observed. We label the microstate of

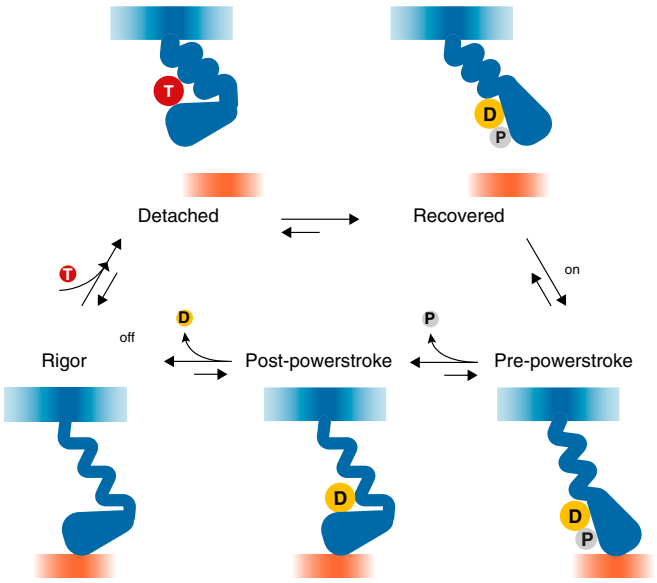

Fig. 2. The myosin II chemomechanical cycle. The myosin thick filament and individual motors are shown in blue; the actin thin filament is shown in orange. Also shown are ATP (T), ADP (D), and inorganic phosphate, P_i (P). Starting from the unbound, recovered state (*Upper Right*), myosin II (with ADP and P_i) binds actin in a pre-power stroke state. Myosin II then releases P_i and performs its power stroke, in which the lever arm rotates to pull the actin filament left against an external load. Myosin II releases ADP to complete the final part of its stroke and to transition to the rigor state. Upon binding ATP, myosin II releases the actin filament. The motor performs its recovery stroke along with ATP hydrolysis. The rate-limiting step of this cycle is ADP release, which is sensitive to the force felt by the myosin II motor.

the system as $\mathbf{n} = (n_{\text{prePS}}, n_{\text{midPS}}, n_{\text{postPS}}, n_{\text{det}}, n_{\text{rec}})$, where n is the number of motors in the state given in the subscript.

A key feature of the model is that it captures the average distribution of strain values across bound motors. Each microstate $\mathbf{n}$ has a unique set of strain values that we calculate assuming that the strain on a pair of consecutive motors differs by a constant $\Delta y(\mathbf{n})$, as if the motors had bound at regular time intervals. For motor i, $y_i(\mathbf{n}, F) = i\Delta y(\mathbf{n}, F) + d_i$, where $d_i = 0, d/2$, and d for a motor in the pre-power stroke, mid-power stroke, and post-power stroke states, respectively. Cutting the stroke in half is a simplification; the second component is slightly smaller in reality (24).

We use Eq. **2** to solve for the strain y_i and because it is proportional to strain, for the slip distance of each motor:

$$\begin{aligned}\Delta x_{\text{slip}}(i, \mathbf{n}, F) &= \frac{y_i(\mathbf{n}, F)}{N-1} \\ &= \frac{i}{(N-1)\sigma_N}\left(\frac{F}{k_{\text{m}}} - n_{\text{midPS}}\frac{d}{2} - n_{\text{postPS}}\, d\right) \\ &\quad + \frac{d}{N-1},\end{aligned} \tag{4}$$

where $\sigma_N = N(N+1)/2$, and $i \in [n_{\text{pre-PS}} + n_{\text{mid-PS}} + 1, N]$ is the index of the post-power stroke motor. In the following results, this expression is used to lend insight into how Δx_{slip} depends on variables like the motor index i, the number of bound motors N, etc.

Our expressions for strain and slip distance assume that, in between motor transitions, the actin filament is in a position given by the balance of forces (Eq. **2**). This neglects fluctuations in the actin filament position due to thermal noise. This and our approximation that the strain values differ by a constant Δy will lead to an error of $\approx \Delta y$ in the strain of any particular motor. We do not expect this to impact our results, which depend primarily on the full range of strain values across all bound motors. The full range is one to two orders of magnitude larger than Δy and is accurately captured. *SI Appendix*, section 1.D has details of the strain model.

This elastic strain model enables an analytical solution that we can rapidly solve over a large number of possible

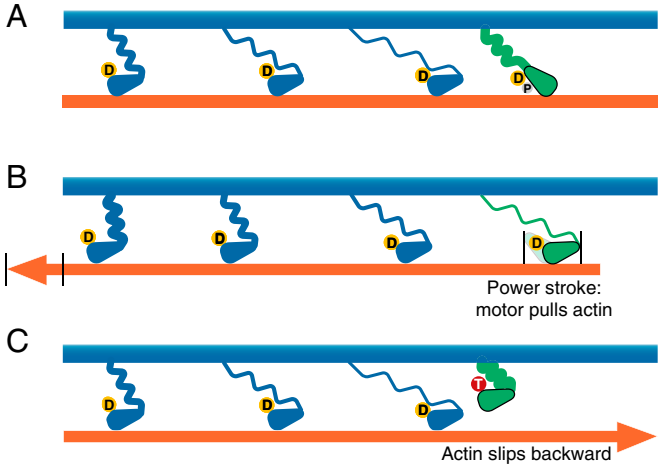

Fig. 3. The mechanism of actin filament sliding in which a motor in the pre-power stroke state (green) releases phosphate and performs its power stroke (A → B), pulling actin to the left and relieving the strain on all other post-power stroke motors (blue). When a post-power stroke motor releases (B → C), the actin filament slides backward a distance proportional to that motor's strain. If the green motor releases first, the slip distance will be large. If the leftmost motor releases first, the slip distance will be small. D, ADP; P, P_i; T, ATP.

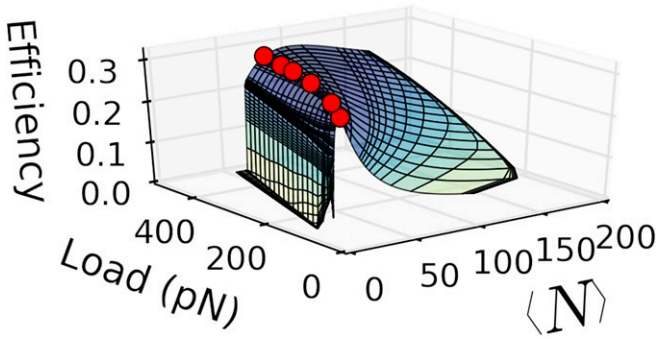

Fig. 4. The efficiency of skeletal muscle contraction as a function of the average number of bound motors $\langle N \rangle$ at different values of external load F. The red dots are the experimentally observed values of $\langle N \rangle$ shown in Fig. 1.

microstates $\mathbf{n}$. For example, limiting our calculations to $N \leq 150$ bound motors (a safe assumption under the conditions studied here), there are 585,275 unique combinations of bound motors $(n_{\text{prePS}}, n_{\text{midPS}}, n_{\text{postPS}})$. To calculate steady-state properties, we solve for the microstate distribution $P(\mathbf{n}|F)$ (*SI Appendix*, section 1.B). The distribution depends on the external load F, which is experimentally controllable. We can then calculate the average number of bound motors as

$$\langle N \rangle = \sum_{\mathbf{n}} P(\mathbf{n}|F) N \delta_{N,\mathbf{n}}, \tag{5}$$

where we have defined the Kronecker delta $\delta_{N,\mathbf{n}}$ to equal one when $N = n_{\text{prePS}} + n_{\text{midPS}} + n_{\text{postPS}}$ and zero otherwise.

A motor that completes one cycle of ATP hydrolysis pulls the actin filament a net distance of $\Delta x_{\text{net}} = \Delta x_{\text{step}} - \Delta x_{\text{slip}}$, where $\Delta x_{\text{step}} = d/N$. The velocity of the actin filament is

$$V(F) = \sum_{\mathbf{n}} J(\mathbf{n}, F) \Delta x_{\text{net}}(\mathbf{n}, F), \tag{6}$$

where $J(\mathbf{n}, F)$ is the flux of and $\Delta x_{\text{net}}(\mathbf{n}, F)$ the net stroke size of post-power stroke motors releasing from microstate $\mathbf{n}$. As we describe in *SI Appendix*, section 1.C, $\Delta x_{\text{net}}(\mathbf{n}, F)$ in Eq. **6** is an average both over motor indices i within microstate $\mathbf{n}$ for the slip distance and over all possible values of $\Delta x_{\text{step}} = d/N$ since the post-power stroke motors in microstate $\mathbf{n}$ may have performed their power strokes with N motors bound, $N-1$ motors bound, etc.

Over the entire system, the average net stroke size is

$$\langle \Delta x_{\text{net}} \rangle = \frac{\sum_{\mathbf{n}} J(\mathbf{n}, F) \Delta x_{\text{net}}(\mathbf{n}, F)}{\sum_{\mathbf{n}} J(\mathbf{n}, F)}, \tag{7}$$

and the thermodynamic efficiency of the half filament is

$$\eta(F) = \frac{F \langle \Delta x_{\text{net}} \rangle}{\Delta \mu_{\text{ATP}}}, \tag{8}$$

where the numerator $F\Delta x$ is the average work done on the actin filament for one full motor cycle and the denominator $\Delta \mu_{\text{ATP}} > 0$ is the free energy gained from hydrolyzing one molecule of ATP.

We parameterize this model from data of Piazzesi et al. (11) for 1) the average number of bound motors $\langle N \rangle$ (Fig. 1), 2) the sliding velocity, and 3) the average net stroke distance $\langle N \Delta x_{\text{net}} \rangle$, all as functions of external load (*SI Appendix*, section 1.G). In the following sections, we use this model to study the speed and efficiency of muscle contraction over different evolutionary degrees of freedom.

Myosin II Motors Have Evolved to Coordinate Their Actions in Order to Optimize Muscle Contraction

Evolution Tunes the Number of Bound Motors to Maximize Efficiency. How does muscle performance depend on the number of bound motors? We vary the on rate of the myosin II model, which alters $\langle N \rangle$ while leaving all other myosin II properties unchanged (*SI Appendix*, section 2 has details).

Fig. 4 shows the model prediction for how muscle efficiency depends on the number of bound motors at different values of external load. We show this in the form of a fitness landscape. The red points show the experimental data of Fig. 1. Because the data coincide with the peak ridge of the model's efficiency landscape, it implies that $\langle N \rangle$ has evolved to optimize efficiency.

Here is the physical interpretation of this optimization. First, if too many motors are bound to the track ($N > \langle N \rangle_{\text{opt}}$), the system is inefficient because more motors than necessary are performing their chemomechanical cycles, and more ATP is being burned. Second, if too few motors are bound ($N < \langle N \rangle_{\text{opt}}$), then the actin backsliding Δx_{slip} is large, as expressed by Eq. **4**. There is a steep drop to zero efficiency, which happens when $\langle \Delta x_{\text{slip}} \rangle \geq \langle \Delta x_{\text{step}} \rangle$, and the system loses all productive motion. The fitness with respect to $\langle N \rangle$ is predicted to be a balance of these two forces, which gives the optimal efficiency.

A Strong Myosin II Power Stroke Is Crucial to Muscle Speed and Efficiency. The power stroke of myosin II generates the force and motion that leads to muscle contraction. The power stroke happens when the motor releases inorganic phosphate and undergoes a rapid conformational change that swings the lever arm and pulls the actin filament (15, 18). In our model, the strength of the power stroke depends on the free energy bias from the pre-power stroke to the post-power stroke state, g_{ps}. Because the bound transitions of myosin II are much faster than the binding and unbinding rates, our model assumes bound motors are in a quasi-equilibrium between the pre-power stroke and post-power stroke states. Thus, a stronger power stroke (more negative value of g_{PS}) corresponds to a greater proportion of motors in the post-power stroke state.

How does muscle performance depend on the strength, g_{ps}, of the power stroke? Fig. 5 shows that a strong power stroke (very negative g_{ps}) gives the greatest efficiency; *SI Appendix*, section 2.A has calculation details and a discussion of the optimal value of g_{PS}. A strong power stroke also gives greater sliding velocity and power output (*SI Appendix*, Fig. S5).

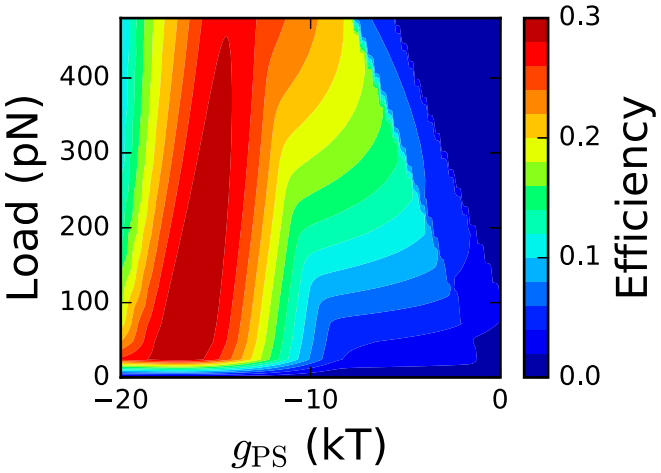

Fig. 5. The efficiency (contour colors) vs. power stroke bias, g_{PS}, at different values of external load. A large and negative g_{PS} greatly improves skeletal muscle efficiency.

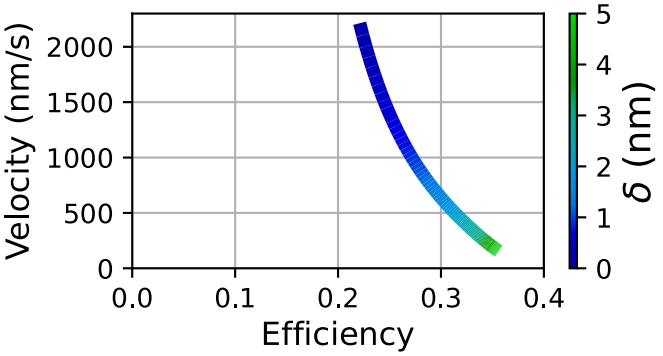

Fig. 6. The speed–efficiency trade-off for actomyosin with respect to force sensitivity of the motor's release from actin δ at $F = 240$ pN. This is a parametric curve: δ is the independent variable; both the velocity and efficiency are dependent variables. With a small force sensitivity δ, more motors are able to release, increasing the speed of the system. However, the net productive motion $\langle \Delta x_{\text{net}} \rangle$ per ATP is small, so the efficiency is low. With a high force sensitivity, only a few motors—those that have been bound longest—can release. This decreases velocity but increases $\langle \Delta x_{\text{net}} \rangle$ and the efficiency.

The explanation for these trends is that a strong power stroke minimizes the actin slip distance Δx_{slip}. When N motors are bound, it is better to have as many of those motors in the post-power stroke state as possible. A motor in the post-power stroke state generates the most force, and a greater number will better share the load. Each individual motor thus has a smaller strain and gives a smaller slip distance (Eq. **4** and *SI Appendix*, Fig. S6). This leads to higher efficiency, velocity, and power output. In *SI Appendix*, section 2.A, we describe that these results give insight into why fatigued muscle has lower efficiency and are important in a broader context for understanding the power stroke mechanism in other molecular machines, not just myosin II.

A Force-Sensitive Off Rate Increases Efficiency at the Expense of Sliding Velocity. Another evolutionary variable that can affect muscle performance is the force sensitivity of the rate at which myosin II releases from actin (Eq. **3**). To study this, we varied the parameter δ while simultaneously controlling the on and off rates to ensure that the average number of motors $\langle N \rangle$ stays constant. This allows us to study the role of force sensitivity without conflating any effect from changing $\langle N \rangle$ (*SI Appendix*, section 2 has details).

Fig. 6 shows the prediction that a larger force sensitivity leads to more efficient muscle contraction. This is because a strong force sensitivity prevents those motors with the greatest strain—and therefore, the greatest actin slip—from releasing. With a strong force sensitivity (large δ), the farthest right (green) motor in Fig. 3 has a large Δx_{slip} but a slow off rate, while the farthest left motor has a small Δx_{slip} and fast off rate. *SI Appendix*, Fig. S4 illustrates how the slip distance Δx_{slip} varies across bound motors.

However, greater efficiency comes at the expense of velocity because the system has to wait around for the correct motor to release. Alternatively, if force sensitivity were small, motors would release quickly and independently. Consider again the green motor in Fig. 3. If this motor has a fast off rate, it will increase the velocity of the system, as long as the net stroke size Δx_{net} is positive, even if it is very small. This motor's release will decrease efficiency, of course, since it lowers the average work ($F \langle \Delta x_{\text{net}} \rangle$) per ATP hydrolyzed (Eq. **8**).

Differences in Speed and Efficiency across Muscle Tissues Can Be Explained by a Few Evolutionary Variables

In nature, there are different myosin II isoforms, ranging from those in slow, efficient skeletal muscle to those in fast, less

efficient skeletal muscle (32–35). The origin of these differences is not fully understood. Our model and the above results give an explanation based on evolutionary control of the strength of the power stroke and the magnitude of the force sensitivity of myosin II.

To explain, we start from the experimental observation that, across different isoforms, the maximum sliding velocity is proportional to the dissociation constant of ADP K_{AD} (32–34, 36). ADP release is force sensitive, and it is the rate-limiting step of the myosin II cycle (Eq. **3** and Fig. 2). In addition, slow, efficient isoforms are known to have a high force sensitivity δ, while fast, inefficient isoforms have low force sensitivity (35, 36).

For our model, we assume that differences to the ADP binding affinity are not a direct cause of changes to speed and efficiency but are a result of changes to g_{PS} or δ. A more efficient system will have a higher binding affinity (smaller K_{AD}) either because the free energy well of the power stroke g_{PS} is deeper, as described by Purcell et al. (33), or because it is required by a higher force sensitivity δ. Therefore, we treat g_{PS} and δ as evolutionary variables. Varying these two quantities in our model captures the differences in speed and efficiency observed across different muscle tissues (Fig. 7). The model also makes two predictions.

First, the model predicts that there are two properties of actomyosin that control the speed–efficiency trade-off: More efficient muscle should have filaments with a smaller number of bound motors $\langle N \rangle$ and with a smaller average slip distance $\langle \Delta x_{slip} \rangle$. Recall that the efficiency, Eq. **8**, is proportional to the average productive motion of a cycle:

$$\eta = \frac{F\,\langle \Delta x_{net} \rangle}{\Delta \mu_{ATP}} = \frac{F}{\Delta \mu_{ATP}} \left(\left\langle \frac{d}{N} \right\rangle - \langle \Delta x_{slip} \rangle \right), \quad [9]$$

where $\Delta x_{step} = d/N$. Eq. **9** shows that efficiency is higher when there are fewer bound motors ($\langle \frac{d}{N} \rangle$ is larger) and when the slip distance Δx_{slip} is smaller.

Second, the model predicts how evolutionary variables of myosin II—the strength of the power stroke g_{PS} and the force sensitivity δ—control these changes in $\langle N \rangle$ and $\langle \Delta x_{slip} \rangle$. In particular, in order to use a smaller number of bound motors $\langle N \rangle$, myosin II needs to have a stronger power stroke g_{PS}. At constant load F, a system with 5 post-power stroke motors has a greater elastic energy than a system with 10 post-power stroke motors. This greater elastic energy can be overcome with a stronger power stroke.

However, all else being equal, a smaller $\langle N \rangle$ will lead to greater actin backsliding Δx_{slip}, as shown in Eq. **4** and Fig. 1. To compensate and reduce $\langle \Delta x_{slip} \rangle$, the more efficient systems have a stronger force sensitivity δ, which ensures that only those motors with small Δx_{slip} release. We also find that, in order to reproduce the data in Fig. 7, our model must assume that more efficient systems have a tighter myosin II stiffness k_m, which further reduces the strain and the slip distance (Eq. **4**).

It is beyond the scope of the model and the available experimental data to give quantitative predictions for g_{PS}, δ, and k_m over different isoforms. Our goal is to predict general trends. We compute these trends with two free parameters for changes to δ and k_m across isoforms. Changes to g_{PS} are calculated with no parameters by assuming the free energy well at the end of the power stroke matches the changes measured by K_{AD} (33). This constraint leads to a trend line in Fig. 7*A* that rises more steeply than the experimental data. Relaxing this constraint and adding a free parameter for changes in g_{PS} would likely give a better fit to the data; we decide against this to avoid overfitting. Also, our model captures the correct trend in Fig. 7*B*, but our efficiency values need to be scaled by a constant factor 1.55 to match the experimental efficiencies. This is because our model predicts slightly smaller values of work on the actin filament and because the experimental values, which are estimated rather than directly measured, assume a different value of $\Delta \mu_{ATP}$ than we use here. *SI Appendix*, section 2.B has specific details of these calculations and trends across the data in Fig. 7.

Conclusions

We have used a dynamical model to understand how myosin II motors coordinate their actions in muscle contraction. A key aspect of actomyosin performance is the distance a

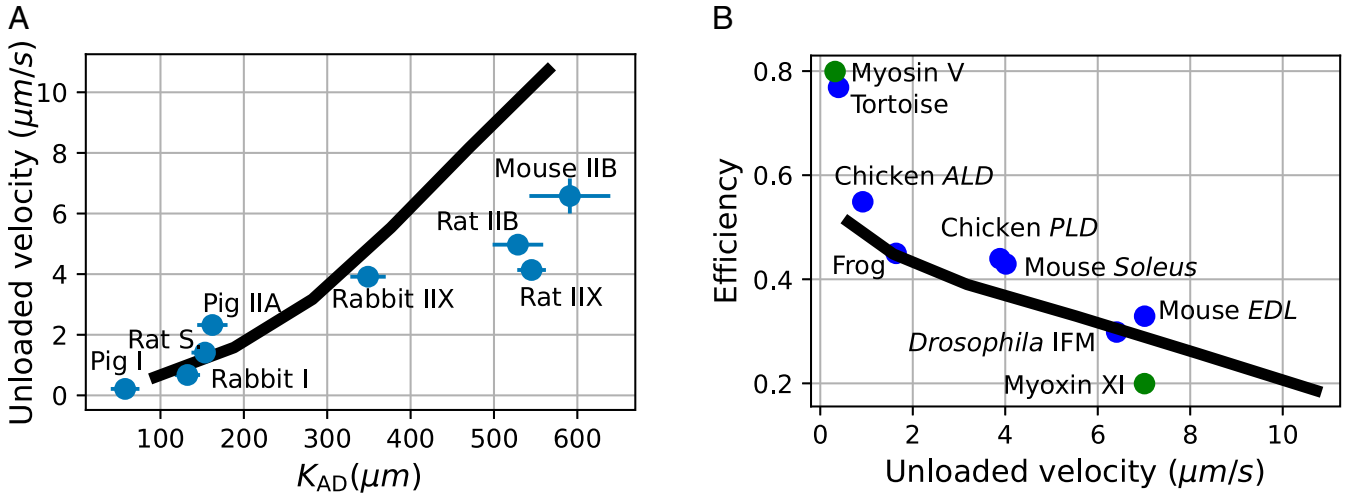

Fig. 7. The speed–efficiency trade-off across muscle tissues. The trend lines show the speed and efficiency of our actomyosin model under evolutionary changes to the strength of the power stroke g_{PS}, the force sensitivity δ, and the myosin II elasticity k_m, as described in the text. We take K_{AD} to be the independent variable since it is experimentally measurable for different myosin II isoforms. Over the displayed range $K_{AD} \in [94, 564]\,\mu$mol, we vary g_{PS} logarithmically from −15.7 to −13.9 kT, k_m linearly from 1.7 to 0.7 pN/nm, and δ linearly from 1.5 to 0.5 nm (*SI Appendix*, section 2.B). (*A*) Our model fit to data from Nyitrai et al. (32) for unloaded shortening velocity vs. K_{AD} for myosin isoforms from different species. (*B*) Our model fit to data taken from Purcell et al. (33) for unloaded shortening velocity vs. efficiency for skeletal muscle tissues (blue): tortoise (*rectus femoris*), chicken (*anterior latissimus dorsi*) (ALD), frog (*sartorius*), chicken (*posterior latissimus dorsi*) (PLD), mouse (*soleus*), (*Drosophila*) adult indirect flight muscle (IFM), and mouse (*extensor digitorum muscle*) (EDM). Also shown in green, for reference, are data from nonmuscle myosin V and myosin XI.

filament slides backward when a motor releases. This backsliding distance is not a property of an individual motor but of the multimotor system as a whole. Our modeling suggests that evolution has reduced backsliding by optimizing the number of bound motors, the strength of the power stroke, and the force sensitivity of myosin II release. The model explains the speed–efficiency trade-off that is observed across different muscle tissues. These results help explain how evolution controls the microscopic physical properties of myosin II proteins in order to optimize the macroscopic properties of muscle contraction.

Data Availability. All study data are included in the article and/or *SI Appendix*.

ACKNOWLEDGMENTS. We are grateful for support from the Laufer Center for Physical and Quantitative Biology.

1. A. I. Brown, D. A. Sivak, Allocating dissipation across a molecular machine cycle to maximize flux. *Proc. Natl. Acad. Sci. U.S.A.* **114**, 11057–11062 (2017).
2. J. A. Wagoner, K. A. Dill, Mechanisms for achieving high speed and efficiency in molecular machines. *Proc. Natl. Acad. Sci. U.S.A.* **116**, 5902–5907 (2019).
3. J. A. Wagoner, K. A. Dill, Opposing pressures of speed and efficiency guide the evolution of molecular machines. *Mol. Biol. Evol.* **36**, 2813–2822 (2019).
4. W. J. Albery, J. R. Knowles, Efficiency and evolution of enzyme catalysis. *Angew. Chem. Int. Ed. Engl.* **16**, 285–293 (1977).
5. T. Schmiedl, U. Seifert, Stochastic thermodynamics of chemical reaction networks. *J. Chem. Phys.* **126**, 044101 (2007).
6. A. I. Brown, D. A. Sivak, Allocating and splitting free energy to maximize molecular machine flux. *J. Phys. Chem. B* **122**, 1387–1393 (2018).
7. A. K. S. Kasper, D. A. Sivak, Modeling work-speed-accuracy trade-offs in a stochastic rotary machine. *Phys. Rev. E* **101**, 032110 (2020).
8. G. Oster, H. Wang, Reverse engineering a protein: The mechanochemistry of ATP synthase. *Biochim. Biophys. Acta* **1458**, 482–510 (2000).
9. J. A. Wagoner, K. A. Dill, Molecular motors: Power strokes outperform Brownian ratchets. *J. Phys. Chem. B* **120**, 6327–6336 (2016).
10. M. J. Greenberg, G. Arpağ, E. Tüzel, E. M. Ostap, A perspective on the role of myosins as mechanosensors. *Biophys. J.* **110**, 2568–2576 (2016).
11. G. Piazzesi *et al.*, Skeletal muscle performance determined by modulation of number of myosin motors rather than motor force or stroke size. *Cell* **131**, 784–795 (2007).
12. H. Huxley, Electron microscope studies of the organisation of the filaments in striated muscle. *Biochim. Biophys. Acta* **12**, 387–394 (1953).
13. A. F. Huxley, R. Niedergerke, Structural changes in muscle during contraction; interference microscopy of living muscle fibres. *Nature* **173**, 971–973 (1954).
14. E. Eisenberg, T. L. Hill, A cross-bridge model of muscle contraction. *Prog. Biophys. Mol. Bio.* **33**, 55–82 (1979).
15. R. Cooke, K. C. Holmes, The mechanism of muscle contraction. *Crit. Rev. Biochem. Mol.* **21**, 53–118 (1986).
16. L. Fusi, E. Brunello, M. Reconditi, G. Piazzesi, V. Lombardi, The non-linear elasticity of the muscle sarcomere and the compliance of myosin motors. *J. Physiol.* **592**, 1109–1118 (2014).
17. M. Caremani, L. Melli, M. Dolfi, V. Lombardi, M. Linari, Force and number of myosin motors during muscle shortening and the coupling with the release of the ATP hydrolysis products. *J. Physiol.* **593**, 3313–3332 (2015).
18. A. Houdusse, H. L. Sweeney, How myosin generates force on actin filaments. *Trends Biochem. Sci.* **41**, 989–997 (2016).
19. M. Kaya, H. Higuchi, Nonlinear elasticity and an 8-nm working stroke of single myosin molecules in myofilaments. *Science* **329**, 686–689 (2010).
20. B. Guo, W. H. Guilford, Mechanics of actomyosin bonds in different nucleotide states are tuned to muscle contraction. *Proc. Natl. Acad. Sci. U.S.A.* **103**, 9844–9849 (2006).
21. C. Veigel, J. E. Molloy, S. Schmitz, J. Kendrick-Jones, Load-dependent kinetics of force production by smooth muscle myosin measured with optical tweezers. *Nat. Chem. Biol.* **5**, 980–986 (2003).
22. M. Kovács, K. Thirumurugan, P. J. Knight, J. R. Sellers, Load-dependent mechanism of nonmuscle myosin 2. *Proc. Natl. Acad. Sci. U.S.A.* **104**, 9994–9999 (2007).
23. E. M. De La Cruz, E. M. Ostap, Relating biochemistry and function in the myosin superfamily. *Curr. Opin. Cell Biol.* **16**, 61–67 (2004).
24. M. Kaya, Y. Tani, T. Washio, T. Hisada, H. Higuchi, Coordinated force generation of skeletal myosins in myofilaments through motor coupling. *Nat. Commun.* **8**, 16036 (2017).
25. S. Walcott, D. M. Warshaw, E. P. Debold, Mechanical coupling between myosin molecules causes differences between ensemble and single-molecule measurements. *Biophys. J.* **103**, 501–510 (2012).
26. S. Stam, J. Alberts, M. L. Gardel, E. Munro, Isoforms confer characteristic force generation and mechanosensation by myosin II filaments. *Biophys. J.* **108**, 1997–2006 (2015).
27. L. Marcucci, T. Washio, T. Yanagida, Including thermal fluctuations in actomyosin stable states increases the predicted force per motor and macroscopic efficiency in muscle modelling. *PLoS Comput. Biol.* **12**, e1005083 (2016).
28. M. Linari, G. Piazzesi, V. Lombardi, The effect of myofilament compliance on kinetics of force generation by myosin motors in muscle. *Biophys. J.* **96**, 583–592 (2009).
29. M. Caremani, L. Melli, M. Dolfi, V. Lombardi, M. Linari, The working stroke of the myosin II motor in muscle is not tightly coupled to release of orthophosphate from its active site. *J. Physiol.* **591**, 5187–5205 (2013).
30. T. Erdmann, U. S. Schwarz, Stochastic force generation by small ensembles of myosin II motors. *Phys. Rev. Lett.* **108**, 188101 (2012).
31. T. Erdmann, P. J. Albert, U. S. Schwarz, Stochastic dynamics of small ensembles of non-processive molecular motors: The parallel cluster model. *J. Chem. Phys.* **139**, 175104–175128 (2013).
32. M. Nyitrai *et al.*, What limits the velocity of fast-skeletal muscle contraction in mammals? *J. Mol. Biol.* **355**, 432–442 (2006).
33. T. J. Purcell *et al.*, Nucleotide pocket thermodynamics measured by EPR reveal how energy partitioning relates myosin speed to efficiency. *J. Mol. Biol.* **407**, 79–91 (2011).
34. J. Walklate, Z. Ujfalusi, M. A. Geeves, Myosin isoforms and the mechanochemical cross-bridge cycle. *J. Exp. Biol.* **219**, 168–174 (2016).
35. M. J. Bloemink, M. A. Geeves, Shaking the myosin family tree: Biochemical kinetics defines four types of myosin motor. *Semin. Cell Dev. Biol.* **22**, 961–967 (2011).
36. K. C. Holmes, D. R. Trentham, R. Simmons, M. Nyitrai, M. A. Geeves, Adenosine diphosphate and strain sensitivity in myosin motors. *Phil. Trans. R. Soc. B* **359**, 1867–1877 (2004).